J. Appl. Comput. Mech., 6(SI) (2020) 1283-1292
DOI: 10.22055/JACM.2020.33496.2237

ISSN: 2383-4536
jacm.scu.ac.ir

Shahid Chamran University of Ahvaz

Journal of Applied and Computational Mechanics

Research Paper

The Brick Thermal Performance Improvement using Phase Change Materials

Nadezhda S. Bondareva[1], Mikhail A. Sheremet[2], Fu-Yun Zhao[3]

[1] Laboratory on Convective Heat and Mass Transfer, Tomsk State University, 36 Lenin Avenue, Tomsk, 634050, Russia, Email: bondarevans@mail.tsu.ru

[2] Laboratory on Convective Heat and Mass Transfer, Tomsk State University, 36 Lenin Avenue, Tomsk, 634050, Russia, Email: sheremet@math.tsu.ru

[3] School of Power and Mechanical Engineering, Wuhan University, Luo-Jia-Shan, Wuhan, 430072, China, Email: fyzhao@whu.edu.cn

Received May 05 2020; Revised May 12 2020; Accepted for publication May 13 2020.
Corresponding author: M.A. Sheremet (sheremet@math.tsu.ru)

Abstract. The problems of heat and mass transfer in phase change materials are of great engineering interest. The absorption and storage of energy in the form of latent heat makes it possible to use them in the construction industry to smooth out the effects of temperature transitions in the environment. This work is devoted to the study of heat transfer in a building block with paraffin inserts under unsteady external conditions. The influence of the geometric dimensions of the block and the volume fraction of the phase change material on the effect of restraining external temperature fluctuations was studied. The unsteady conjugate melting problem was solved in a closed rectangular region with two cavities filled with PCM. The temperature of the environment on the left boundary changes in harmonic law. Thermal distributions were obtained at various points in time.

Keywords: Latent heat; Energy efficiency; Building; Finite difference method.

1. Introduction

Modern problems associated with increased electricity consumption and the problems of global warming and climate change in large cities [1] pose the tasks of a more rational use of energy resources. The need for renewable energy and its optimal storage appears [2–4]. The introduction of materials with low melting points in building materials and blocks can significantly reduce energy costs spent on air conditioning systems. Latent melting energy increases the effective heat capacity of the structure and reduces the temperature fluctuations inside the room caused by daily changes in ambient temperature. Periodic temperature fluctuations contributing to the periodic melting and solidification of the material leads to inertia of the heat exchange processes between the external environment and the room.

The inclusion of such materials in walls, roofs, windows, and other structural elements can be carried out in several ways: adding inserts, impregnating a structural element, encapsulation, etc. Materials are selected in accordance with the following requirements: characteristic features of phase transitions, high latent heat, suitable thermal conductivity, high density and low thermal expansion coefficient, chemical stability, non-toxicity and not flammable [5]. Low thermal conductivity improves thermal resistance of the structure. Such materials include various salt solutions, paraffins, waxes, fatty acids, etc. In particular, paraffins are not susceptible to subcooling, corrosion, and have a wide range of melting points.

Climatic characteristics of the environment of use impose restrictions on the choice of material: the main properties that affect productivity, are the thermal properties of PCM, since the absorption and release of energy occurs when passing through the melting point [6–10]. As weather conditions are changed during the seasons, PCM based designs will have the greatest benefit in some months and the least benefit in other months. It should also be noted that for each climatic zone, it is worthwhile to select the suitable material based on its properties, as well as the conditions that must be maintained inside the building.

The processes occurring in such structures are studied experimentally and numerically [10–15]. High interest is associated with the possibility of reducing heat loss of the building and energy costs. So in [15] it was experimentally shown that adding PCM to a brick leads to a 15% reduction in energy consumption. One-dimensional approximation was used to estimate heat loss in a four-story building through PCM-based walls and ceilings, as well as concrete foundations [16]. The weather conditions of different cities of the subarctic climate were considered. It was found that in the case of an addition of a PCM layer of 10 mm the energy savings reaches 9852 kWh, while with a layer of 50 mm up to 15837 kWh.

Eicosane with T_m = 35 °C (L_F = 160 kJ/kg) embedded bricks for cooling of building in Deli were considered experimentally [17]. It was shown that a temperature decrease of more than 9.5 °C is achieved by adding two layers of PCM, while the heat gain can be reduced by 60%. Peak temperatures can be reduced to 7° [18]. In [19] the effectiveness of using microencapsulated PCM to reduce temperature fluctuations in asphalt and, as a result, reduce cracking at low temperatures was demonstrated.

Much attention should be paid to the thermophysical properties of PCM and solid construction material. The thermal interaction of structural layers significantly affects the application efficiency of PCM. Influence of location PCM layer in multi–

Published online: August 27 2020

layer wall was evaluated in an experimental study [20]. A decrease in heat flux on the inner surface was noted when adding PCM. Maximum decrease in the heat flux 10.7% observed with inclusion PCM closer to the internal medium at maximum ambient temperatures T_{max} = 64.6 °C. At maximum temperatures T_{max} = 51 ˚C a 6.7% decrease in heat flux was observed at the location of PCM between the middle layers of insulation.

Numerical study of PCM container as an outer or inner layer in the concrete based wall was carried out in [6]. One-dimensional conjugate problem of melting and solidification was solved at different positions of PCM layers. It was shown that the optimal thickness (from 1 to 20 mm) and the melting temperature depend on the climatic conditions of the place of use and varies with the month. For three different cities, the most optimal melting points for material selection were determined. The addition of PCM to the design allowed energy savings of up to 18% depending on climate and season.

Pasupathy and Velraj [21] considered a one-dimensional roof model with inclusion of PCM with the melting temperature range 26° – 28°C as an intermediate layer with a 2.5 cm thickness. External layer of brick was 10 cm, and an inner 12cm layer of concrete. The temperature changes of each individual layer were monitored over time. It was shown that the addition of PCM significantly reduces the daily temperature fluctuations in the layers, while in the concrete layer, coupled conjugated with the internal environment, the temperature remains at the same level of 27°C in the winter months, when the surface temperature of the outer layer varies from 21°C to 40°C. Bhamare et al. [22] considered a three-dimensional model of a room with a layered roof as presented in experimental study [21]. In numerical study, it was also noted that phase transitions reduce peak thermal loads, it was shown that the melting and solidification processes maintain the ceiling temperature near the melting temperature of 25.5° ≤ T ≤ 27.5°C. The influence of the angle of the roof was also investigated and the maximum reduction in heat gain (by 16%) was found at an inclination angle of 2°. Natural convection in the melt also has a large effect on heat transfer [23]. With the free movement of the melt, it is necessary to study the thermal interaction of the flow and structural elements depending on the geometric and thermal characteristics. Some interesting results for heat transfer performance of phase change materials can be found in [24–26].

In the present research, the model of a rectangular brick with PCM inserts, which plays the role of a partition between an environment with an unsteady temperature and a room with a constant temperature with periodic changes in external thermal conditions, was considered. A numerical study of unsteady processes of conjugate heat transfer taking into account phase transitions is carried out. The Oberbeck–Boussinesq equations in dimensionless stream function, vorticity, and temperature, were formulated.

2. Mathematical Model

An unsteady conjugate heat and mass transfer problem inside a rectangular block 3L × 5L with local rectangular inserts of a phase change material is considered (Figure 1). The conditions of convective heat exchange with the environment are established on the left and right walls, while the upper and lower boundaries are thermally insulated. The ambient temperature at the left wall changes in harmonic law, the air temperature from the right wall was constant and below the melting temperature. Rectangular bricks with different PCM volume: solid brick without PCM (case 1), and rectangular PCM inserts (Figure 1a) of size: 0.5L × 1L (case 2), 1L × 1L (case 3) and 1.5L × 1.5L (case 4). Figure 1b shows a physical model with with local square inserts L×L (case 3) in detail.

It was considered that the region is elongated in depth and the longitudinal dimension of the inserts is much longer than the dimensions of the cross section, so as to use the two-dimensional approximation. As a phase change material, n-octadecane with a melting point of T_F = 28.05 °C is used. The block material has the properties of a brick with thermal conductivity k = 0.7 W/(mK). At the initial time, paraffin was in a solid state, the temperature in the entire region, was below the melting point of paraffin.

Inside the brick under consideration, the heat conduction equation is solved:

$$\frac{\partial h}{\partial t} = k_B\left(\frac{\partial^2 T}{\partial x^2} + \frac{\partial^2 T}{\partial y^2}\right) \tag{1}$$

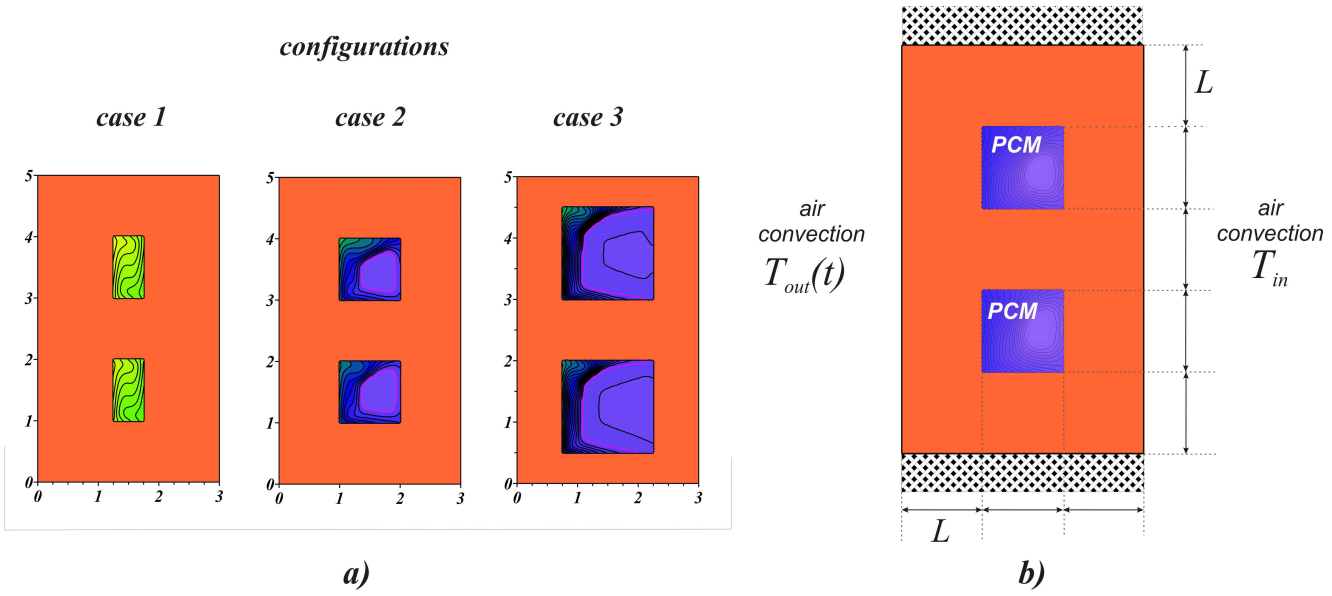

Fig. 1. The configurations of the brick under consideration (*a*), and basic configuration (case 3) of the brick: a rectangular brick block with square paraffin inserts (*b*).

Heat transfer inside the phase change material is carried out not only due to heat conduction, phase transitions and natural convection in the melt should also be taken into account. To describe the buoyancy forces in a viscous Newtonian fluid, the Boussinesq condition was used. Since the frequency of changes in the external temperature was very low, the temperature differences were small and the dimensions of the cavities were considered small (1 cm ≤ L ≤ 4 cm) so the laminar flow regime was considered. In this formulation, the process of mass, momentum and energy transfer is described by a system of non-stationary two-dimensional Oberbeck – Boussinesq convection equations using primitive variables "velocity – pressure – enthalpy" [27, 28]:

$$\frac{\partial u}{\partial x}+\frac{\partial v}{\partial y}=0 \tag{2}$$

$$\rho\left(\frac{\partial u}{\partial t}+u\frac{\partial u}{\partial x}+v\frac{\partial u}{\partial y}\right)=-\frac{\partial p}{\partial x}+\mu\left(\frac{\partial^2 u}{\partial x^2}+\frac{\partial^2 u}{\partial y^2}\right) \tag{3}$$

$$\rho\left(\frac{\partial v}{\partial t}+u\frac{\partial v}{\partial x}+v\frac{\partial v}{\partial y}\right)=-\frac{\partial p}{\partial y}+\mu\left(\frac{\partial^2 v}{\partial x^2}+\frac{\partial^2 v}{\partial y^2}\right)+\rho\beta g(T-T_F) \tag{4}$$

$$\frac{\partial h}{\partial t}+u\frac{\partial h}{\partial x}+v\frac{\partial h}{\partial y}=k_l\left(\frac{\partial^2 T}{\partial x^2}+\frac{\partial^2 T}{\partial y^2}\right) \tag{5}$$

The equation of energy transfer in paraffin wax:

$$\frac{\partial h}{\partial t}=k_s\left(\frac{\partial^2 T}{\partial x^2}+\frac{\partial^2 T}{\partial y^2}\right) \tag{6}$$

Here the enthalpy is determined by temperature and depends on the phase state as follows:

$$h=\begin{cases}\rho_s c_s T, & T<T_F,\\ \rho_s c_s T_F+\rho_l L_F+\rho_l c_l(T-T_F), & T\geq T_F.\end{cases}$$

As a characteristic scale, the linear size of the inserts filled with paraffin (L) was chosen; the remaining thermophysical characteristics were recorded taking into account the following relationships:

$$X=x/L,\ Y=y/L,\ V_0=\sqrt{g\beta(T_H-T_F)L},\ U=u/V_0,\ V=v/V_0,\ \tau=tV_0/L,$$
$$\Theta=(T-T_F)/(T_H-T_F),\ \Psi=\psi/(V_0L),\ \Omega=\omega L/V_0$$

Here T_H is the maximum ambient temperature.

The considered system of equations was solved using dimensionless stream function, vorticity and temperature. The hydrodynamic equations for the melt employing the non-primitive variables will take the following form:

$$\frac{\partial^2\Psi}{\partial X^2}+\frac{\partial^2\Psi}{\partial Y^2}=-\Omega \tag{7}$$

$$\frac{\partial\Omega}{\partial\tau}+U\frac{\partial\Omega}{\partial X}+V\frac{\partial\Omega}{\partial Y}=\sqrt{\frac{Pr}{Ra}}\left(\frac{\partial^2\Omega}{\partial X^2}+\frac{\partial^2\Omega}{\partial Y^2}\right)+\frac{\partial\Theta}{\partial X} \tag{8}$$

From the definition of enthalpy, it follows that any displacement of the interphase boundary is accompanied by the release or absorption of energy, which must be taken into account when solving equation (5). To simplify the process of modeling heat dissipation near the interface, a smoothing function φ was introduced [27, 28]:

$$\varphi=\begin{cases}0, & \Theta<-\eta\\ \dfrac{\Theta-\eta}{2\eta}, & \eta\leq\Theta\leq\eta\\ 1, & \Theta>\eta\end{cases}$$

Here, η is the smoothing parameter and it equals to 0.01.

To solve the energy equation, auxiliary functions were also introduced $\xi(\varphi)$ and $\zeta(\varphi)$ characterizing the changes in thermal conductivities and volumetric heat capacities depending on the volume of the melt, respectively:

$$\xi(\varphi)=\frac{k_s}{k_l}+\varphi\left(1-\frac{k_s}{k_l}\right),\quad \zeta(\varphi)=\frac{\rho_s c_s}{\rho_l c_l}+\varphi\left(1-\frac{\rho_s c_s}{\rho_l c_l}\right)$$

The energy equation for PCM taking into accounts the phase transitions and natural convection takes the form:

$$\zeta(\varphi)\left[\frac{\partial\Theta}{\partial\tau}+U+V\frac{\partial\Theta}{\partial Y}\right]+Ste\cdot\left[\frac{\partial\varphi}{\partial\tau}+U\frac{\partial\varphi}{\partial X}+V\frac{\partial\varphi}{\partial Y}\right]=\frac{\xi(\varphi)}{\sqrt{Ra\cdot Pr}}\left(\frac{\partial^2\Theta}{\partial X^2}+\frac{\partial^2\Theta}{\partial Y^2}\right). \tag{9}$$

For a brick material, the dimensionless heat conduction equation takes the form:

$$\frac{\partial\Theta}{\partial\tau}=\frac{\alpha_B/\alpha_{PCM}}{\sqrt{Ra\cdot Pr}}\left(\frac{\partial^2\Theta}{\partial X^2}+\frac{\partial^2\Theta}{\partial Y^2}\right) \tag{10}$$

At time moment τ = 0, the temperature inside the block, including paraffin inserts, was lower than the melting temperature of the material Θ_0 = -0.1, and since the material was in the solid state, the values of the stream function and vorticity were zero Ψ = 0, Ω = 0. As the boundary conditions in a dimensionless form for the presented statement of the problem were as follows:

- At the borders between different components of the system: $k_1 \frac{\partial \Theta_1}{\partial \overline{n}} = k_0 \frac{\partial \Theta_0}{\partial \overline{n}}$;
- On the left border with the environment: $X = 0$, $0 \le Y \le 5$: $\left.\frac{\partial \Theta}{\partial X}\right|_M = -Bi(\Theta_M - \Theta_{out})$, where $\Theta_{out} = \sin\left(\frac{2\pi\tau}{2P}\right)$ (P is dimensionless half-cycle equivalent to 12 hours in dimensional time);
- On the right border: $X = 3$, $0 \le Y \le 5$: $\left.\frac{\partial \Theta}{\partial X}\right|_M = -Bi(\Theta_M - \Theta_{in})$, where $\Theta_{in} = 0.1$;
- On horizontal surfaces: $0 \le X \le 3$, $Y = 0$ and $Y = 5$: $\frac{\partial \Theta}{\partial Y} = 0$.

Boundary conditions for the Poisson equation for the stream function and the vorticity dispersion equation are $\Psi = 0$ and $\Omega = -\nabla^2 \Psi$ that have been used for all solid boundaries of the melt region, including the interphase border.

3. Validation of the Numerical Algorithm

Partial differential equations (7)–(10) were solved using the finite-difference method [27, 28]. Parabolic equations for the vorticity and temperature were solved using the locally one-dimensional Samarskii scheme. It should be noted that the energy conservation equation for PCM was solved without isolating the liquid and solid zone of paraffin. At the same time, the momentum equation and the Poisson equations for the stream function were solved in the melt region, which is determined on each time layer through the temperature field. To determine the field of the stream function, the method of successive over relaxation was applied.

The obtained numerical scheme was tested on a number of experimental and numerical works [27, 28]. The superposition of isotherms obtained numerically on a black and white photograph of the experimental setup [29] is shown in Figure 2. In the experimental study [29], a rectangular region containing an aluminum substrate with longitudinal aluminum fins and filled with lauric acid inside was considered. The wall opposite the slab and the side walls were thermally insulated by acrylic material. Slab was heated by heat transfer fluid at a constant temperature. The effect of the angle of inclination of the region, as well as the number of edges on the phase transitions of the acid, was investigated. In addition, the measuring temperature with thermocouples, the position of the melting front at various points in time was recorded using the images. Figure 2 shows the case when the angle of inclination is 90 with one fin at time instants t = 45 minutes and t = 75 minutes.

For studied statement of the problem the grid convergence of the solution was investigated. Figure 3 shows the results obtained on grids 60 × 120, 120 × 200, 180 × 300 and 240 × 400. Figure 3a shows isotherms and a phase transition line (pink) for different grids. It is seen that the isotherms on the grids 120 × 200, 180 × 300 and 240 × 400 differ slightly, and on the grids 180 × 300 and 240 × 400 (black dash and black solid line) it practically coincide. The same results are observed as a function of the volume of the melt and time. Interphase boundaries for each grid also coincide. The calculations were carried out on a rectangular uniform grid of dimension 120 × 200. Inside the PCM cavities, 40 × 40 nodes were located.

4. Results and Discussion

In this study, the heat transfer problem was considered taking into account phase transitions and natural convection in the melt under unsteady external thermal conditions. As a result of the calculations, detailed temperature distributions in the material, velocity fields in the melt at fixed times were obtained, and the influence of the wall thickness and PCM volume fraction on the temperature of the brick block was analyzed. Physical properties of the considered media are presented in Table 1.

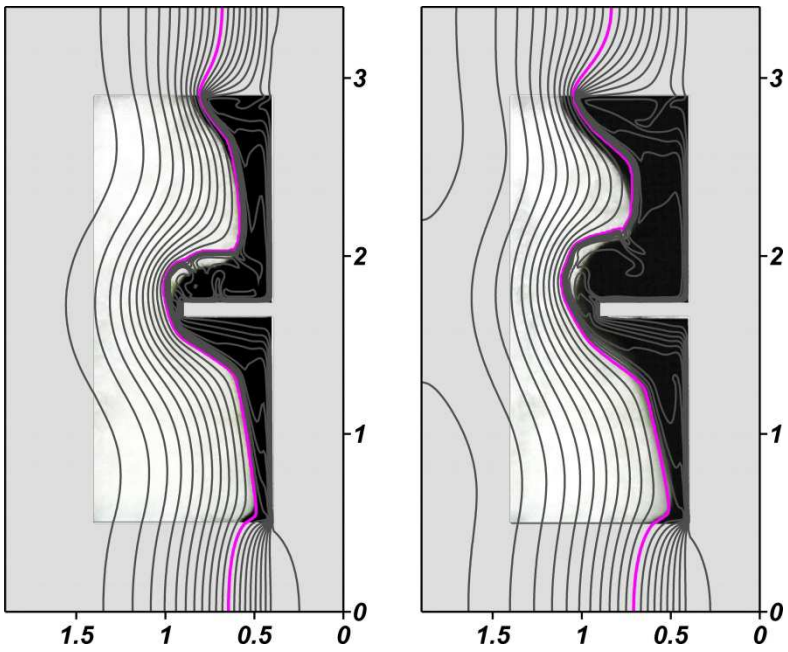

Fig. 2. Comparison of calculated data with experimental results of Kamkari and Groulx [29]: black fill - molten PCM and white fill - solid PC M. Isotherms and phase transition line (color) are obtained numerically.

Table 1. Properties of the working materials.

Properties	Brick [30]	PCM [31]	
		solid	liquid
α, $m^2\ s^{-1}$	$5.2\cdot10^{-7}$	$2.5\cdot10^{-7}$	$9.2\cdot10^{-8}$
K, W/(m·K)	0.7	0.39	0.157
c, J/(kg·K)	840	1900	2200
ρ, kg/m^3	1600	814	770
μ, Pa·s	–	–	$3.8\cdot10^{-3}$
L_F	–	$2.41\cdot10^5$	

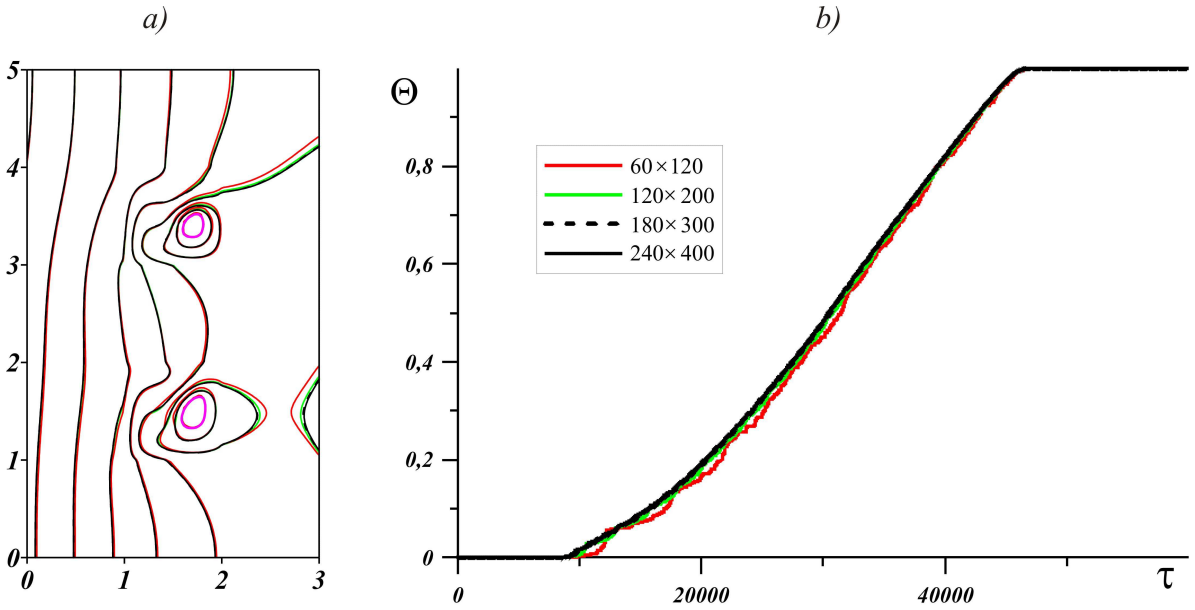

Fig. 3. Isotherms Θ (*a*) and evolution of the liquid volume fraction (*b*) for $Ra = 9.96\cdot10^4$.

The temperature of the medium from the side of the left wall of the region changed according to a harmonic law. In the time period presented, the temperature of the environment Θ_{out} increased from 0 to 1, and then decreased to zero again. The temperature of the medium to the right of the brick was constant and $\Theta_{in} = -0.1$. Heat transfer coefficient on the left wall was equal $\gamma_{out} = 10$ W/(mK), on the right wall $\gamma_{in} = 5$ W/(mK). At the initial moment of time, the temperature of the brick and material coincided with Θ_{in}.

Figure 4 shows the temperature fields at different times for different Rayleigh numbers $Ra = 9.96\cdot10^4$, $Ra = 7.97\cdot10^5$, $Ra = 2.69\cdot10^6$, $Ra = 6.37\cdot10^6$, which corresponds to the characteristic dimensions of the inserts $L = 1$ cm, $L = 2$ cm, $L = 3$ cm and $L = 4$ cm, respectively.

At time $t = 3$ hours, it is evident that, due to higher thermal conductivity, a curvature of temperature isolines and isotherms condense to paraffin inserts are observed in the brick. The isotherm $\Theta = 0$ reaches the brick cavities in which the melting process begins. At low Rayleigh numbers ($Ra = 9.96\cdot10^4$) for a period of time when $\Theta_{out} > 0$, the paraffin has time to completely melt, while on the right wall related to the room, the maximum temperature of all the cases considered is observed. A growth of the Rayleigh number leads to slowing down the melting process, however, the left side warms up evenly and in Figures 4*c* and 4*d* the temperature fields to the left of the PCM differ slightly. At time 9 hours and 12 hours, isothermal displacement is observed. With an increase in the melt region, natural convection develops in the cavities, as a result, the warmer melt rises.

At lower Rayleigh numbers, the region under consideration warms up more intensively. Figure 5 shows the dependence of the average temperature Θ_{avg} on the left and right walls for different Rayleigh numbers, where Θ_{avg} was calculated for walls $X = 0$ and $X = 3$ over the entire height of the block. The left wall temperature monotonously increases with increasing ambient temperature. In this case, with an increase in the Rayleigh number, heating occurs faster and the wall temperature is higher. In the case of $Ra = 9.96\cdot10^4$, in the middle of the process, the temperature begins to rise abruptly, which is associated with the end of the melting process.

The greatest effect of the melting process is observed on the right wall, where an intense increase in temperature occurs until the melting temperature is reached. Further on the graphs it can be seen the inflection corresponding to the beginning of the melting of the material. In the case of lower Rayleigh number, the earlier the material begins to melt. This moment is characterized by the temperature Θ_{avg} in a gentle mode, since in the process of melting paraffin absorbs a large amount of energy and this inhibits the temperature increase. The temperature goes to a smoother mode and for Rayleigh numbers $Ra \geq 7.97\cdot10^5$ it does not significantly exceed the melting point of paraffin during the entire heating period, while at $Ra = 9.96\cdot10^4$ in the last stages the temperature of the right border is heated intensively, like the outer border at $Ra = 6.37\cdot10^6$. Thus, Θ_{avg} on the right wall is more than 0.4 larger than Θ_{avg} for other Rayleigh numbers.

Peak ambient temperatures will be observed at $t = 6$ hours, however, maximum temperatures on the right wall of the brick are observed at about time $t = 9$ hours for all considered Rayleigh numbers. Table 2 presents the average values of Θ at the lateral boundaries. It can be seen that an increase in the Rayleigh number from $Ra = 9.96\cdot10^4$ to $Ra = 7.97\cdot10^5$ reduces the temperature from 0.421 to 0.031, which contributes to a significant decrease in heat transfer with the air in the room, however, a further increase in the Rayleigh number affects Θ_{avg} slightly.

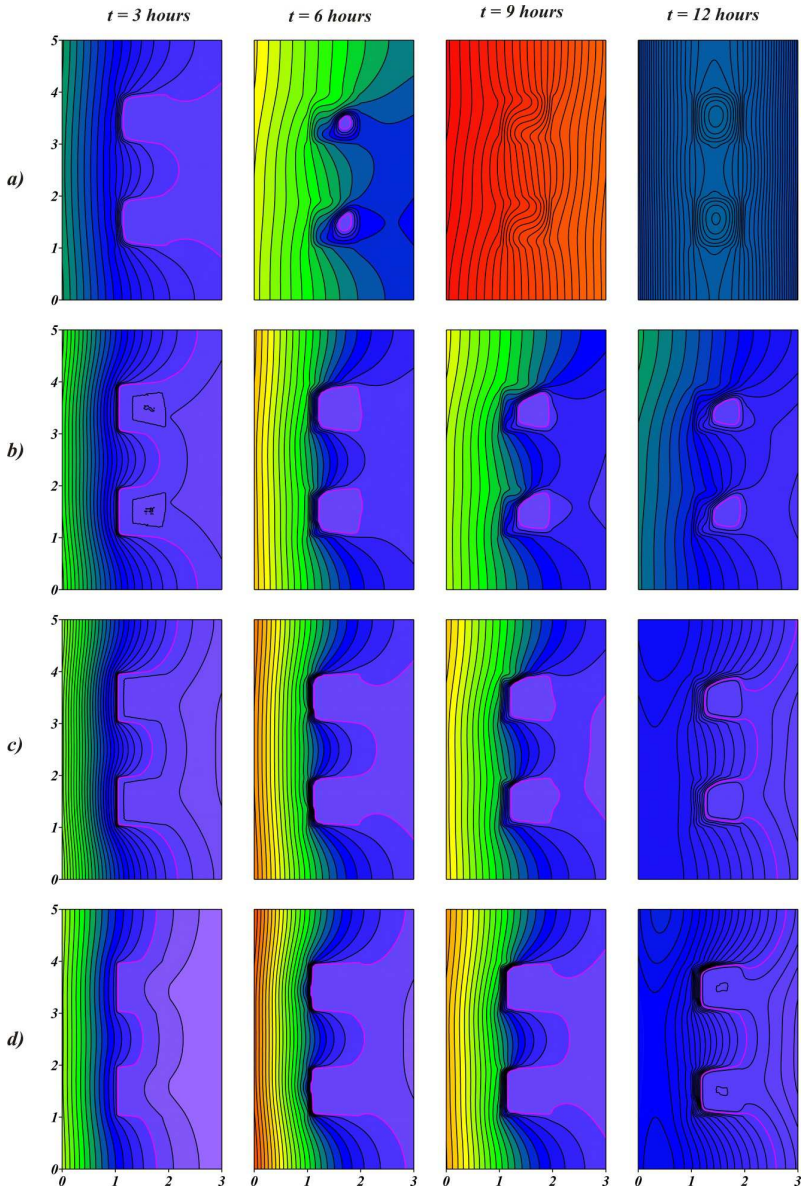

Fig. 4. Temperature fields inside the block at different Rayleigh numbers: a) $Ra=9.96\times10^4$, b) $Ra=7.97\times10^5$, c) $Ra=2.69\times10^6$, d) $Ra=6.37\times10^6$.

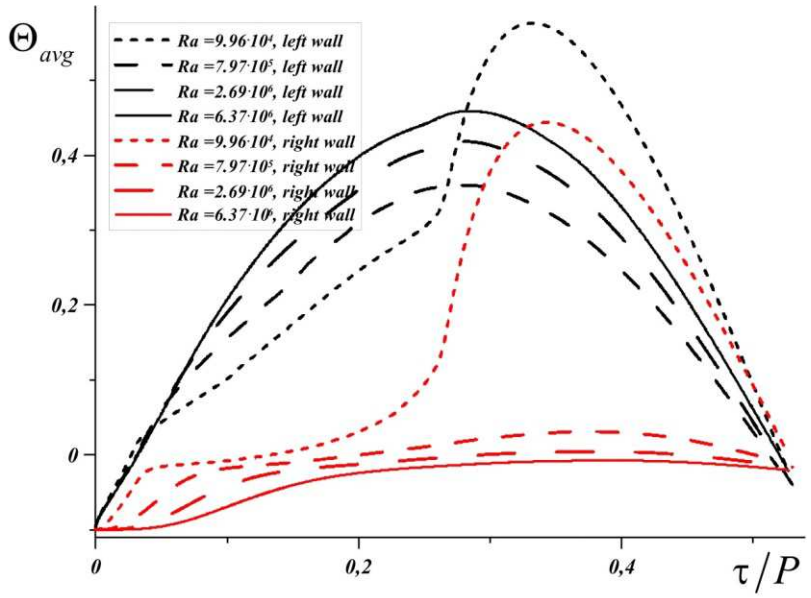

Fig. 5. Average temperature on the left wall versus time for different values of the Rayleigh number.

Table 2. Average wall temperatures at for different Rayleigh numbers.

	t, hours	*Ra*			
		9.96×10^4	7.97×10^5	2.69×10^6	6.37×10^6
Left wall	3	0.138	0.194	0.24	0.268
	6	0.305	0.354	0.407	0.441
	9	0.528	0.285	0.335	0.379
	12	0.094	0.031	0.044	0.061
Right wall	3	-0.002	-0.014	-0.028	-0.054
	6	0.095	0.011	-0.006	-0.016
	9	0.421	0.031	0.004	-0.008
	12	0.092	0	-0.01	-0.016

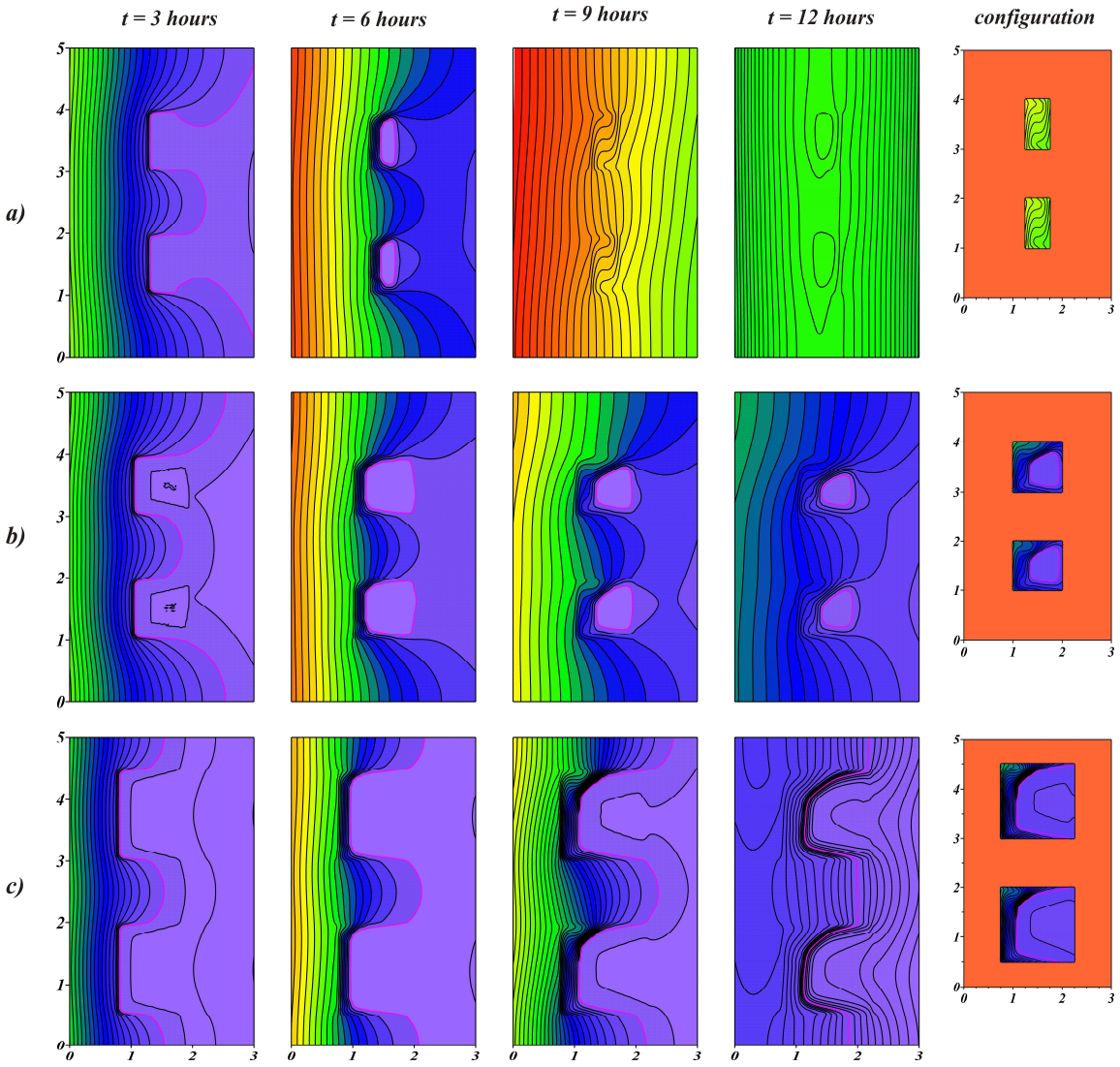

Fig. 6. Effect of PCM volume fraction on temperature fields for $Ra = 7.97\cdot10^5$.

The effect of the paraffin volume fraction with a fixed Rayleigh number $Ra = 7.97\cdot10^5$ on the temperature fields is shown in Figure 6. The sizes of the cells filled with phase change material are 0 (case 1), 0.5 × 1 (case 2), 1 × 1 (case 3) and 1.5 × 1.5 (case 4) in dimensionless units. As with an increase in the Rayleigh number with an increase in the melt volume, the temperature of the right wall rises more slowly. With a small volume of PCM, the material quickly melts and the brick warms up significantly, the dimensionless temperature in paraffin at time t = 9 hours reaches 0.3 (Figure 8*a*). In cases 3 and 4, the material is not completely melted, which is a potential for higher peak temperatures and longer heating. In this case, the temperature profiles in the middle section X = 1.5 show lower values. In the case of V_{PCM} = 1, as with V_{PCM} = 2.25, the minimum temperature values close to 0 and the corresponding regions of the unmelted material are distinguished. You can also observe an increase in temperature with increasing Y. Natural convection heat transfer in the melt contributes to a more intense heating in the upper part of the block. In the case of V_{PCM} = 2.25, the minimum temperatures are observed in the cross section X = 1.5. Also, it should be noted that in this configuration the left wall has the lowest temperature, however, this is due to the absorption of energy during the phase transition. As a result, an increased volume of paraffin contributes to a more intense heat exchange with the external environment and more intense energy absorption. The absorbed heat in the form of latent heat will subsequently be released during the onset of the cold time of day and will help to reduce thermal fluctuations in the room.

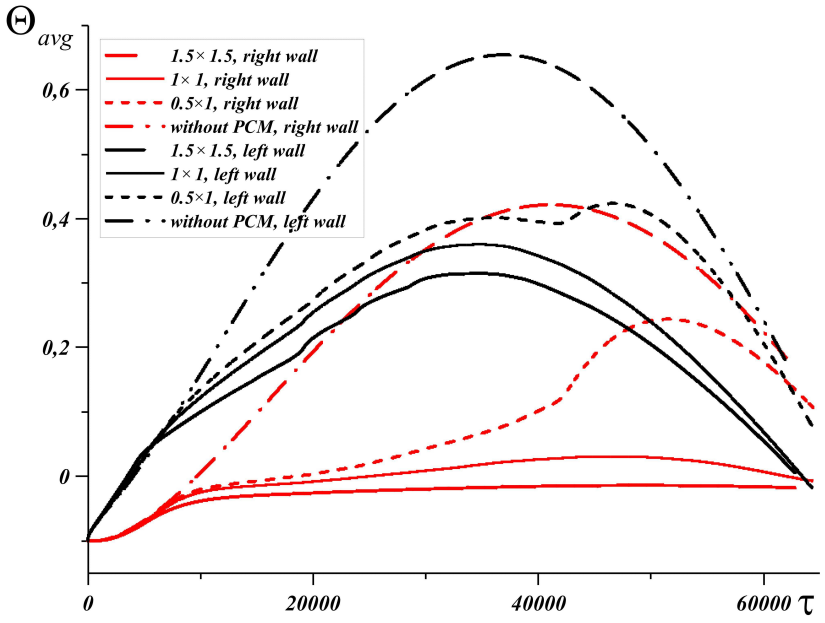

Fig. 7. The average temperature on the right and left walls for different volumes of material for $Ra = 7.97 \cdot 10^5$.

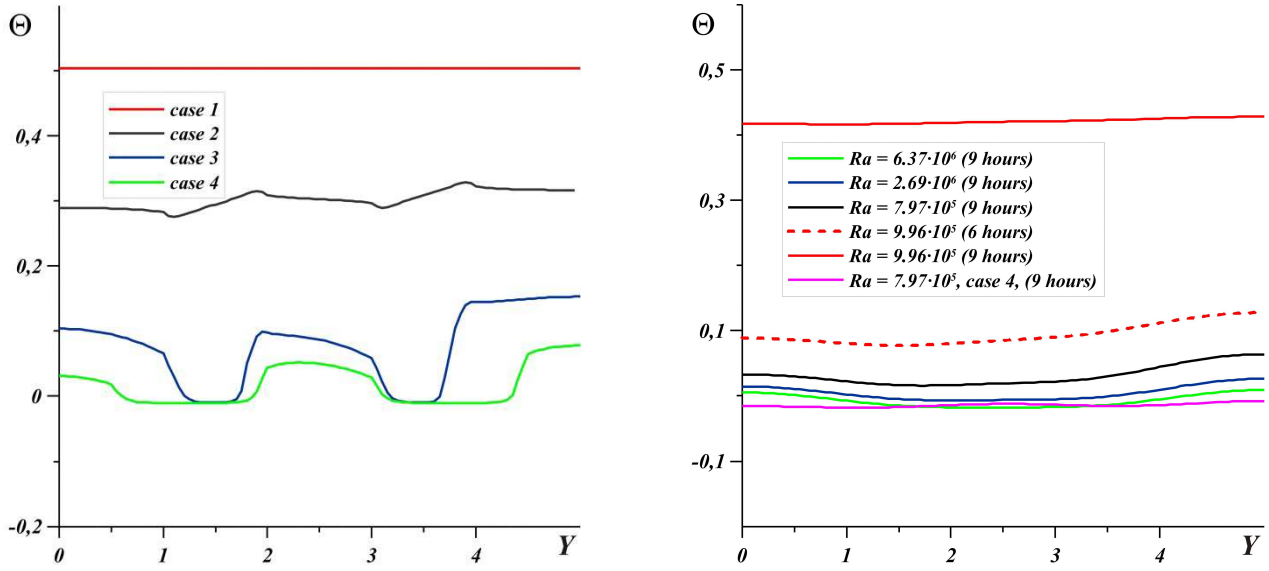

Fig. 8. Temperature profiles in the middle section X = 1.5 at time moment t = 9 hours for different concentrations of PCM (*a*); and temperature profiles on the right wall depending on the Rayleigh number (*b*).

Figure 7 shows the time dependence of the average dimensionless temperature on the left and right walls for different configurations. In a solid brick, without cavities, a uniform monotonous increase in temperature is observed, while the right wall warms up to a value of 0.4, as in the case of $V_{PCM} = 1$ at $Ra = 9.96 \cdot 10^4$.

Figure 8*a* demonstrates the temperature profiles in the middle section for different volumes at time $t = 9$ hours. It can be seen that in the absence of PCM, the brick completely warms up to a dimensionless temperature of 0.5. With the addition of paraffin inserts $V_{PCM} = 0.5$, the region warms up less intensively, while the paraffin melts completely. With an increase in V_{PCM} and an increase in the Rayleigh number (Figs. 8*a* and 8*b*), the effect of natural convection is detected. The upper part of the brick warms up more intensively, as the heated melt rises to the upper walls of the enclosures.

Figure 8*b* presents a comparison of temperature profiles on the right wall at time instants $t = 9$ hours for different cases. Comparison of the basic configuration at different Rayleigh numbers and the configuration with the largest PCM fraction showed that increasing the material fraction is as effective as the overall increase in block size (increasing the Rayleigh number). The temperature on the right wall in the case of $V_{PCM} = 2.25$ and $Ra = 7.97 \cdot 10^5$ is slightly lower than with $V_{PCM} = 1$ for $Ra = 2.69 \cdot 10^6$ and $Ra = 6.37 \cdot 10^6$. Thus, from the point of view of reducing thermal loads, an increase in the PCM fraction of 2.25 times led to the same result as an increase in the overall block scale by 4 times.

5. Conclusions

A numerical study of heat and mass transfer processes in a rectangular brick block with paraffin inserts taking into account melting and solidification, as well as convective heat and mass transfer in the melt was carried out. The influence of the characteristic sizes of the brick and the fraction of phase change material on the side walls temperature during heating of the left wall by air convection was analyzed. The melting process of paraffin strongly inhibits the temperature increase on the right wall, however, after the material has completely melted, the wall temperature reaches its maximum value. The brick warms up quickly,

but when the melting point is reached, a large amount of energy is spent on the phase transition, as a result of which the wall temperature, at the border with the space of the room, remains at the level of the melting temperature. At the same time, a large amount of energy is absorbed by the material as latent heat, which will be released when the temperature drops below the melting temperature. The high thermal conductivity of the brick leads to the fact that the region quickly and monotonously warms up, and then also quickly and monotonously cools down, while the dimensionless temperature on the left wall reaches 0.6. An increase in the volume fraction of paraffin in the brick also contributes to an increase in the thermal resistance of the brick. An increase in the volume of the cavity of the block by 2.25 times reduces the effect of warming on the internal space of the building, as well as an increase in the size of bricks and cavities by 4 times. On the other hand, it should be borne in mind that an increase in the volume of the inserts reduces the structural strength.

Author Contributions

N.S. Bondareva conducted the numerical experiments and analyzed the obtained results; M.A. Sheremet planned the scheme, initiated the project and suggested the mathematical model; F.-Y. Zhao discussed the results. The manuscript was written through the contribution of all authors. All authors discussed the results, reviewed and approved the final version of the manuscript.

Conflict of Interest

The authors declared no potential conflicts of interest with respect to the research, authorship and publication of this article.

Funding

The work was supported by the Russian Science Foundation (Project No. 19-79-00308).

Nomenclature

Bi	Biot number [–]	α	Thermal diffusivity [$m^2 \cdot s^{-1}$]
C	Specific heat [$JK^{-1}\ kg^{-1}$]	β	Coefficient of thermal expansion [K^{-1}]
g	Gravitational acceleration [$m \cdot s^{-2}$]	γ	Heat transfer coefficient [$W \cdot m^{-2} \cdot K^{-1}$]
h	Enthalpy [$J \cdot kg^{-1}$]	Θ	Dimensionless temperature [–]
k	Thermal conductivity [$W \cdot m^{-1} \cdot K^{-1}$]	Θ_{avg}	Dimensionless average temperature on the side boundaries [–]
L	Cavity height [m]		
L_F	Fusion energy or latent heat of melting [$J \cdot kg^{-1}$]	μ	Dynamic viscosity [Pa·s]
p	Pressure [Pa]	ν	Kinematic viscosity [$m^2 \cdot s^{-1}$]
P	Dimensionless half-cycle equivalent to 12 hours in dimensional time [–]	ρ	Density [$kg \cdot m^{-3}$]
		τ	Dimensionless time [–]
Pr	Prandtl number [–]	ψ	Stream function [$m^2 \cdot s^{-1}$]
Ra	Rayleigh number [–]	Ψ	Dimensionless stream function [–]
Ste	Stefan number [–]	ω	Vorticity [s^{-1}]
t	Time [s]	Ω	Dimensionless vorticity [–]
T	Temperature [K]		
T_F	Melting temperature [K]		
u, v	Velocity components in Cartesian coordinates along x and y [$m \cdot s^{-1}$]	*Subscripts*	
		B	Brick
U, V	Dimensionless velocity components [–]	l	Liquid
x, y	Dimensional Cartesian coordinates [m]	PCM	Phase change material
X, Y	Dimensionless Cartesian coordinates [–]	s	solid

References

[1] Li, J., Zhang, C., Zheng, X., Chen. Y., Temporal-Spatial Analysis of the Warming Effect of Different Cultivated Land Urbanization of Metropolitan Area in China. *Scientific Reports*, 10, 2020, 2760.
[2] Comello, S., Reichelstein, S., The emergence of cost effective battery storage, *Nature Communications*, 10, 2019, 2038.
[3] Leicester, R., Newman, V., Wright, J., Renewable energy sources and storage, *Nature*, 272, 1978, 518–521.
[4] Caccia, M., Tabandeh-Khorshid, M., Itskos, G. et al., Ceramic–metal composites for heat exchangers in concentrated solar power plants, *Nature*, 562, 2018, 406–409.
[5] Baetens, R., Jelle, B.P., Gustavsen A., Phase change materials for building applications: A state-of-the-art review, *Energy and Buildings*, 42, 2010, 1361-1368.
[6] Arıcı, M., Bilgin, F., Nižetić, S., Karabay, H., PCM integrated to external building walls: An optimization study on maximum activation of latent heat, *Applied Thermal Engineering*, 165, 2020, 114560.
[7] Lagou, A., Kylili, A., Šadauskiene, J., Fokaides, P.A., Numerical investigation of phase change materials (PCM) optimal melting properties and position in building elements under diverse conditions, *Construction and Building Materials*, 225, 2019, 452-464.
[8] Hichem, N., Noureddine, S., Nadia, S., Djamila, D., Experimental and numerical study of a usual brick filled with PCM to improve the thermal inertia of buildings, *Energy Procedia*, 36, 2013, 766-775.
[9] Barreneche, C., Navarro, M.E., Fernández, A.I., Cabeza, L.F., Improvement of the thermal inertia of building materials incorporating PCM. Evaluation in the macroscale, *Applied Energy*, 109, 2013, 428-432.
[10] Yu, J., Yang, Q., Ye, H., Luo, Y., Huang, J., Xu, X., Gang, W., Wang, J., Thermal performance evaluation and optimal design of building roof with outer-layer shape-stabilized PCM, *Renewable Energy*, 145, 2020, 2538-2549.
[11] Alawadhi, E.M., Using phase change materials in window shutter to reduce the solar heat gain. *Energy and Buildings*, 47, 2012, 421-429.
[12] Mehdaoui, F., Hazami, M., Messaouda, A., Taghouti, H., Guizani, A.A., Thermal testing and numerical simulation of PCM wall integrated inside a test cell on a small scale and subjected to the thermal stresses, *Renewable Energy*, 135, 2019, 597-607.
[13] Ziasistania, N., Fazelpour, F., Comparative study of DSF, PV-DSF and PV-DSF/PCM building energy performance considering multiple parameters, *Solar Energy*, 187, 2019, 115-128.
[14] Evers, A.C., Medina, M.A., Fang, Y., Evaluation of the thermal performance of frame walls enhanced with paraffin and hydrated salt phase change materials using a dynamic wall simulator, *Building and Environment*, 45, 2010, 1762-1768.
[15] Castell, A., Martorell, I., Medrano, M., Perez, G., Cabeza, L.F., Experimental study of using PCM in brick constructive solutions for passive cooling, *Energy and Buildings*, 42, 2010, 42, 534-540.

[16] Kenzhekhanov, S., Quantitative evaluation of thermal performance and energy saving potential of the building integrated with PCM in a subarctic climate, *Energy*, 192, 2020, 116607.
[17] Saxena, R., Rakshit, D., Kaushik, S.C., Experimental assessment of Phase Change Material (PCM) embedded bricks for passive conditioning in buildings, *Renewable Energy*, 149, 2019, 587-599.
[18] Saxena, R., Rakshit, D., Kaushik, S.C., Phase change material (PCM) incorporated bricks for energy conservation in composite climate: A sustainable building solution, *Solar Energy*, 183, 2019, 276-284.
[19] Bueno, M., Kakar, M.R., Refaa, Z., Worlitschek, J., Stamatiou, A., Partl M.N., Modification of asphalt mixtures for cold regions using microencapsulated phase change materials, *Scientific Reports*, 9, 2019, 20342.
[20] Jin, X., Medina, M. A., Zhang, X., On the placement of a phase change material thermal shield within the cavity of buildings walls for heat transfer rate reduction, *Energy*, 73, 2014, 780-786.
[21] Pasupathy, A., Velraj, R., Effect of double layer phase change material in building roof for year round thermal management, *Energy and Buildings*, 40, 2008, 193-203.
[22] Bhamare, D.K., Rathod, M.K., Banerjee, J., Numerical model for evaluating thermal performance of residential building roof integrated with inclined phase change material (PCM) layer, *Journal of Building Engineering*, 28, 2020, 101018.
[23] S. Mehryan, A. M., Ayoubi-Ayoubloo, K., Shahabadi, M., Ghalambaz,·M., Talebizadehsardari, P., Chamkha, A. Conjugate phase change heat transfer in an inclined compound cavity partially filled with a porous medium: a deformed mesh approach, *Transport in Porous Media*, 132, 2020, 657–681
[24] Ghalambaz, M., Chamkha, A.J., Wen, D., Natural convective flow and heat transfer of Nano-Encapsulated Phase Change Materials (NEPCMs) in a cavity, *International Journal of Heat and Mass Transfer*, 138, 2019, 738-749.
[25] Mehryan, S.A.M., Tahmasebi, A., Izadi, M., Ghalambaz, M., Melting behavior of phase change materials in the presence of a non-uniform magnetic-field due to two variable magnetic sources, *International Journal of Heat and Mass Transfer*, 149, 2020, 119184.
[26] Ghalambaz, M., Zadeh, S.M.H., Mehryan, S.A.M., Haghparast, A., Zargartalebi, H., Free convection of a suspension containing nano-encapsulated phase change material in a porous cavity; local thermal non-equilibrium model, *Heliyon*, 6, 2020, e03823.
[27] Bondareva, N.S., Sheremet, M.A., Effect of nano-sized heat transfer enhancers on PCM-based heat sink performance at various heat loads, *Nanomaterials*, 10(1), 2019, 17.
[28] Bondareva, N.S., Sheremet, M.A., Effect of inclined magnetic field on natural convection melting in a square cavity with a local heat source, *Journal of Magnetism and Magnetic Materials*, 419, 2016, 476-484.
[29] Kamkari, B., Groulx, D., Experimental investigation of melting behavior of phase change material in finned rectangular enclosures under different inclination angles, *Experimental Thermal and Fluid Science*, 97, 2018, 94-108.
[30] Kant, K., Shukla, A., Sharma, A., Heat transfer studies of building brick containing phase change materials, *Solar Energy*, 155, 2017, 1233-1242.
[31] Benard, C., Gobin, D., Zanoli, A., Moving boundary problem: heat conduction in the solid phase of a phase-change material during melting driven by natural convection in the liquid, *International Journal of Heat and Mass Transfer*, 29(11), 1986, 1669-1681.

ORCID iD

Nadezhda S. Bondareva https://orcid.org/0000-0003-1536-3106
Mikhail A. Sheremet https://orcid.org/0000-0002-4750-0227
Fu-Yun Zhao https://orcid.org/0000-0001-7481-2990

How to cite this article: Bondareva N.S., Sheremet M.A., Zhao F.-Y. The Brick Thermal performance Improvement Using Phase Change Materials, *J. Appl. Comput. Mech.*, 6(SI), 2020, 1283–1292. https://doi.org/10.22055/JACM.2020.33496.2237